

NuSTAR non-x-ray background

Brian W. Grefenstette¹,^{a,*} Kristin K. Madsen¹,^b
Hiromasa Miyasaka¹,^a and Andreas Zoglauer^c

^aCalifornia Institute of Technology, Space Radiation Lab, Pasadena, California, United States

^bNASA Goddard Space Flight Center, CRESST and X-Ray Astrophysics Laboratory,
Greenbelt, Maryland, United States

^cUniversity of California, Space Sciences Laboratory, Berkeley, California, United States

Abstract. We present an overview of the *NuSTAR* non x-ray background. This is dominated by proton scattering in the detector and surrounding material as well as activation lines from of material in the detector and its housing. We also discuss contributions from the solar component (when the Sun is active), and the impact of short-lived radiation belts on the *NuSTAR* background and activation in the detectors. © *The Authors. Published by SPIE under a Creative Commons Attribution 4.0 International License. Distribution or reproduction of this work in whole or in part requires full attribution of the original publication, including its DOI.* [DOI: [10.1117/1.JATIS.8.4.047001](https://doi.org/10.1117/1.JATIS.8.4.047001)]

Keywords: x-ray; background; satellites.

Paper 22069G received Jun. 28, 2022; accepted for publication Nov. 14, 2022; published online Dec. 6, 2022.

1 Introduction

NuSTAR is the first focusing hard x-ray telescope in orbit.¹ At low energies ($E < 20$ keV) the *NuSTAR* background is typically dominated by the cosmic x-ray background (CXB),^{2,3} while at higher energies the background is associated with a variety of different phenomena including stray light from sources outside the field of view (FoV),^{4,5} solar x-rays during flares that can penetrate through the spacecraft, and a non x-ray background (NXB) related to particles or γ -rays hitting the instrument and spacecraft and producing bremsstrahlung/continuum emission. Activation of various materials can also produce time-dependent emission in the form of γ -ray decay lines. *NuSTAR* is in a fairly benign 6 deg-inclination orbit with an altitude typically around 600 km. This prevents extended excursions into the south Atlantic anomaly (SAA). Figure 1 shows the typical spectrum during an observation, which includes the components from the sky as well as the internal background lines.

Each *NuSTAR* focal plane moduel (FPMA and FPMB) of CdZnTe detectors is embedded in CsI anti-coincidence shield, which provides an active veto for charged particles [Fig. 1(b)]. This results in suppression of the background from minimum ionizing particles by vetoing events in the CdZnTe that are coincident with events in the CsI shield. However, this also provides a scattering target that surrounds the detectors so that the NXB effectively originates from all directions. Focused x-rays enter through the Be windows at the top as shown in this cross-section, and are therefore incident on the front face of the detectors. A “depth cut”⁶ can help discriminate background photons from the source photons above ≈ 40 keV. This is applied by default when the data are processed using NuSTARDAS.

Understanding the NXB, its spectral shape, and its variability are key ingredients to constructing any model of the background emission. For most moderately bright *NuSTAR* observations, sources are dominant over the CXB, only becoming comparable to the background at energies $E > 30$ keV, where the NXB is the dominant background component.

In this paper we make use of the entire *NuSTAR* archive through early 2022 to study the evolution of the NXB over the first 10 years of the mission. We show how to mitigate some sources of background (such as the Sun), and investigate the various radiation belts that contribute to the *NuSTAR* NXB.

*Address all correspondence to Brian W. Grefenstette, bwgref@srl.caltech.edu

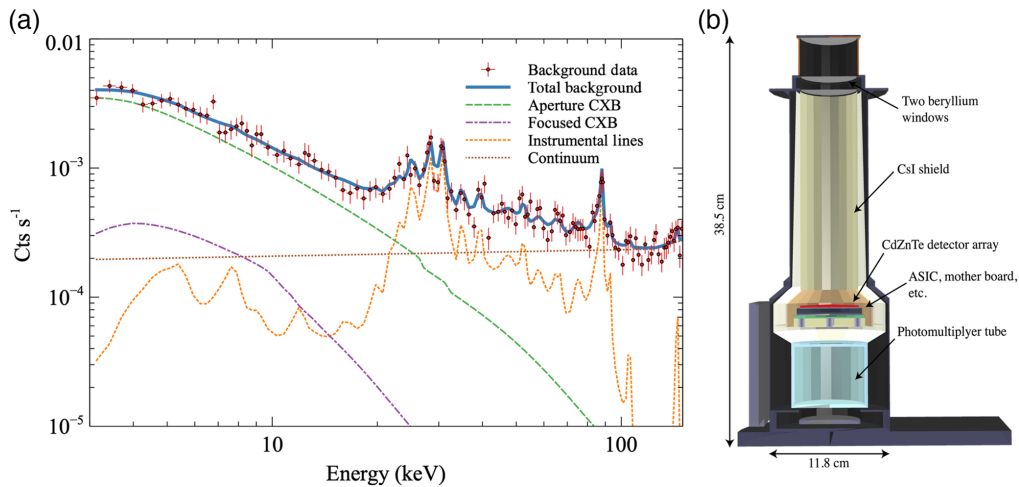


Fig. 1 (a) A typical *NuSTAR* background spectrum during an observation, here taken from the supernova remnant N132D. Data are shown from a source-free region of the FoV and are modeled using the standard `nuskybgd` components: focused (dot-dashed, purple) CXB components, the aperture (or stay light) CXB component (dashed green), the internal background line model (short dashed, orange), and the internal continuum model (dotted, brown). The sun was not active during this observation, so no solar component is present. These combine into the total background model (solid, blue). In this paper we use occulted data to remove the CXB components and concentrate on the internal, NXB components of the background. (b) The geometry of the *NuSTAR* focal plane module used to produce the RMFs in GEANT4. Figure reproduced from Kitaguchi et al.⁶

2 Data and Data Selection

2.1 Occulted Data Extraction

The data used in this paper are extracted from the “cleaned” level 2 event files in the *NuSTAR* archive at the science operations center (SOC). These data have all of the standard NuSTARDAS filters applied to them and are separated into the standard observing “modes.” To remove the sky background, we only use data when the sky is occulted by the Earth. *NuSTAR* does not repoint when the Earth enters the FoV, so in its low-earth (≈ 600 km) orbit the Earth occults the FoV for roughly 30-min out of every 96-min orbit. The duration of this occultation period varies depending on the position of the source in the sky and the time of the observation. By default, the NuSTARDAS pipeline uses the `prefilter` FTOOL⁷ and the *NuSTAR* orbital ephemeris in the two-line element (TLE) file to derive a number of key orbital parameters such as the “elevation” (ELV) of the telescope bore-sight from the Earth limb, whether *NuSTAR* is in sunlight or not (SUNSHINE), and the time since the telescope last exited the SAA. For standard science operations, “occulted” *NuSTAR* data are defined to include all data where the ELV parameter is < 3 deg. In general, this is a conservative estimate to avoid any atmospheric attenuation from the Earth influencing the light curves or spectra of observations. Since we are attempting to remove all source photons from our data sets, we need to be more aggressive.

To estimate the appropriate ELV cutoff, we select data from observations of an extremely bright high-mass x-ray binary (HMXB), A0535 + 26 during outburst. In this state, the source was several times brighter than the Crab, resulting in incident count rates > 2500 counts per second on the *NuSTAR* detectors. We make a plot of the count rate versus the elevation angle (Fig. 2) and see the excess source emission included in the occulted data (ELV < 3 deg).

We also perform a simple check in this case to see if there a discrepancy between the ingress and egress from the Earth limb (which could occur if there was a systematic misalignment between the telescope angle being used by `prefilter` and the actual bore-sight of the telescope). Here it is more convenient to simply plot the instrument livetime (which is inversely proportional to the incident count rate) and the elevation angle versus time (Fig. 3). We do a coarse estimate of the time when the livetime plateaus at its “high” level (when the source

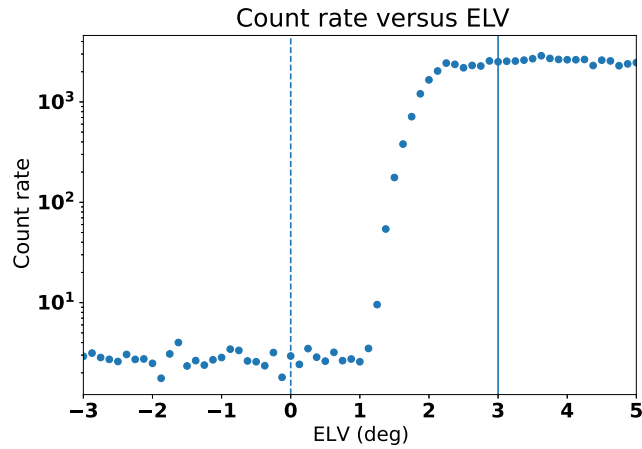


Fig. 2 The livetime-corrected source count rate versus the angle to the Earth limb (ELV). The vertical line shows the standard cutoff for occulted science data, while the vertical dashed line shows the cutoff used in this analysis.

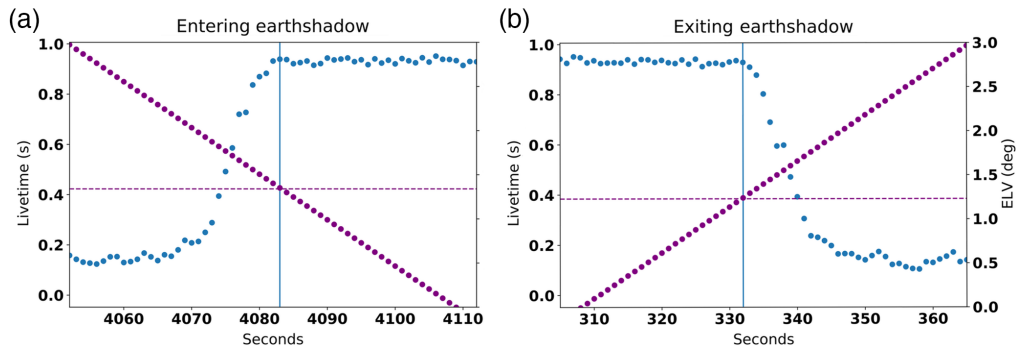


Fig. 3 The data here show the instrument livetime (left axis, blue data points) and the ELV (right axis, purple data points) for (a) an ingress and (b) egress from Earth shadow. The vertical solid line is a by-hand estimation of when the livetime has plateaued, while the horizontal guide line shows the ELV where this occurs. This corresponds to the time when the source is 100% blocked by the Earth limb.

is behind the Earth) and find that both the ingress and egress time periods reach peak livetime at roughly 1.3 deg of ELV. This confirms that there is no systematic uncertainty in the `prefilter` measurement and also that if we use an aggressive ELV cutoff of <0 deg that we will have removed all of the source-related photons from the dataset.

An interesting implication of this analysis is that the ELV cutoff of 3 deg used by `nupipeline` results in at most 40 s of exposure loss before the atmospheric attenuation removes a majority of the source flux. However, if there are impulsive events that are evolving on time-scales of a few seconds it might be possible to extend the usable science data beyond the end of the “SCIENCE” mode data.

2.2 Solar Contamination

X-rays from the Sun can be especially bright when the Sun is active or flaring. To achieve the cleanest data set for our analysis, we want to remove the solar spectrum as it is highly variable and contains x-ray emission lines below 10 keV. A separate analysis dedicated to modeling the solar component in a similar manner to the CXB components is underway.

To estimate the impact of contamination due to solar background we produce monthly-averaged background spectra with $\text{ELV} < 0$ deg. `Prefilter` also provides an estimate of the “orbit day” based on the TLE and solar system ephemeris (via the `SUNSHINE` column). Using

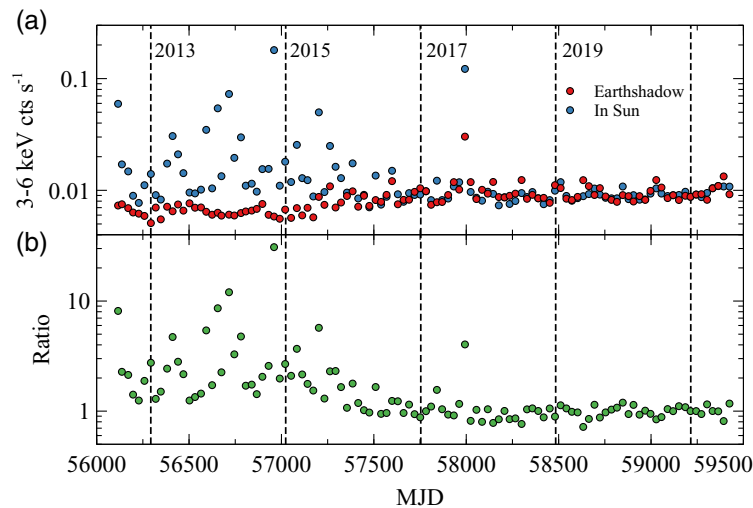


Fig. 4 (a) A comparison of the 3 to 6 keV “In Sun” (blue) and in Earthshadow (red) count rates for the first 100 months since launch showing the excess near solar maximum in 2014 (MJD 56700) and the relative quiet during the recent solar minimum. (b) The ratio of the two rates, showing the high amount of solar activity in the first three years of the mission, as well as the enhanced activity in September 2017 (MJD 58000), during which there were multiple X- and M-class flares.

these data we construct data sets where *NuSTAR* is “in Sun” and “in Earthshadow.” The solar flux is primarily at low energies, so we integrate the monthly spectrum from 3 to 6 keV to estimate the received source rate on “DET0” for FPMA as a proxy for solar activity. We can then look at the difference between the rates in sunlight and in Earthshadow to estimate the impact of solar activity (Fig. 4). The first few years of the *NuSTAR* mission correspond to the peak of the solar cycle, so we see a lot of evidence for enhanced solar activity. We expect to see this activity increase again in the mid-2020s during the next solar maximum. The SUNSHINE flag is only an approximate estimate of whether the observatory is in sunlight based on the TLE. To fully remove the impact of solar activity, we would likely need to “bias” the entry into Earthshadow, similarly to how we use a more conservative cut of the ELV angle above. A more detailed study is beyond the scope of this work; here, we mainly use this to demonstrate the presence of an additional solar background.

We find that up until roughly four years after launch (mid-2016) there is a significant rate of enhanced background that can be associated with solar activity. After that, there are sporadic instances when individual months can be affected (i.e., Month 62 is September 2017 when there were multiple X-class flares).

For individual observations, the enhanced background from solar activity can appear both as “prompt” contribution from the x-ray flares themselves as well as “delayed” emission due to space weather (i.e., particles from a coronal mass ejections, or CMEs, that populate short-lived radiation belts; see Sec. 3.2). For the prompt emission, the x-ray flares can be so bright that the emission can penetrate through all of the shielding surrounding the detectors, even when *NuSTAR* is not pointed near the Sun. An example of this shown in Fig. 5 from an x-class solar flare on March 11, 2015, when *NuSTAR* was pointed 64 deg from the Sun. For situations like this, the *NuSTAR* SOC typically recommends avoiding using any of the data during the flare for science analysis of the primary target; the GOES full-disk integrated x-ray count rates can typically be used to filter out the solar activity, though during peak solar activity it can be difficult to distinguish between *NuSTAR* background spikes due to solar x-ray activity (when GOES is useful) and enhanced radiation belt activity (when GOES is not).

The major difference between these two phenomena is that the solar x-ray events have a thermal spectrum (with emission lines associated with 10 to 100 MK gas in the solar corona), while the radiation belt events show enhancements in the apparent nonthermal background and can dominate the high-energy background spectrum for the entire month. Figure 6 shows representative spectra for each case.

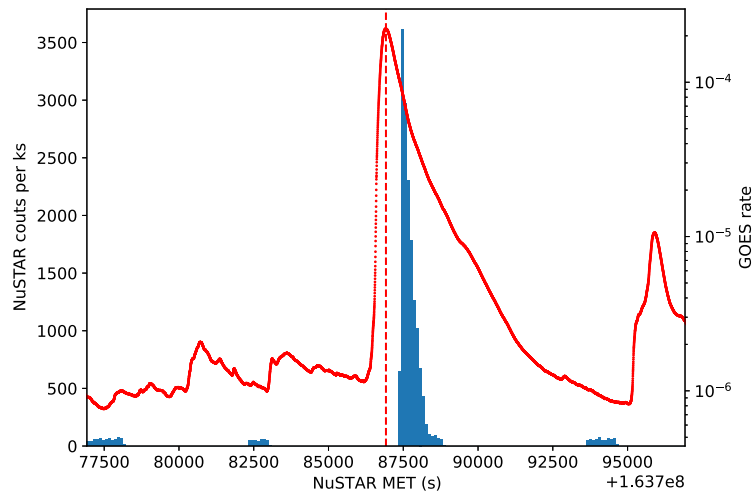


Fig. 5 The enhanced background caused by the X2.1 flare on March 11, 2015, during *NuSTAR* SEQID 30002041014. The blue-filled histogram shows the *NuSTAR* count rate during the flare, while the red trace shows the GOES x-ray flux monitor. The vertical dashed line is the time of the flare. The “missing” *NuSTAR* data here are caused by the event selection criteria and/or when *NuSTAR* was behind the Earth.

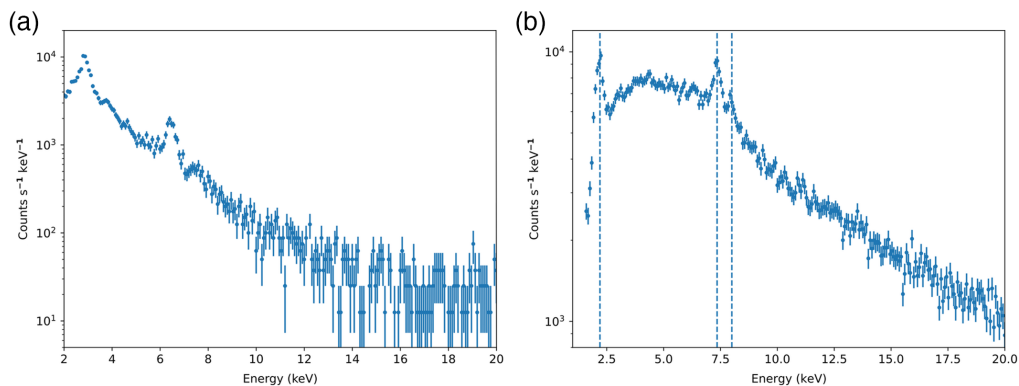


Fig. 6 (a) The observed spectrum of the solar flare shown in Fig. 5 showing the predominantly thermal spectrum along with a Fe emission lines around ~ 6.4 to 6.7 keV as well as emission (presumably from S XXV) at ~ 2.9 keV. (b) The spectrum of an “orphan” spike in the background associated with a radiation belt enhancement from September 08, 2017 during *NuSTAR* SEQID 60301028002 showing the continuum spectrum as well as fluorescence lines associated with the material surrounding the detectors (vertical dashed lines).

Unfortunately, neither of these cases can be systematically mitigated. The SOC provides background maps and lightcurves to help identify cases where automated screening could be used, while the NuMASTER table includes a flag set during the quality assessment of observations to identify observations with enhanced backgrounds due to solar or space weather activity.

3 Geomagnetic Variations

NuSTAR is different from most other high-energy observatories in that its low-inclination orbit avoids extended plunges through the SAA and completely avoids the high-latitude radiation belts. The sidereal drift of the orbit and the precessional period of the orbit (roughly 37 days) combine so that over a calendar month *NuSTAR* samples a majority of the geographic area. During quiet months, this can result in an apparent east/west asymmetry in the observed background. Figure 7 shows that the geographic distribution of the background strength mirrors

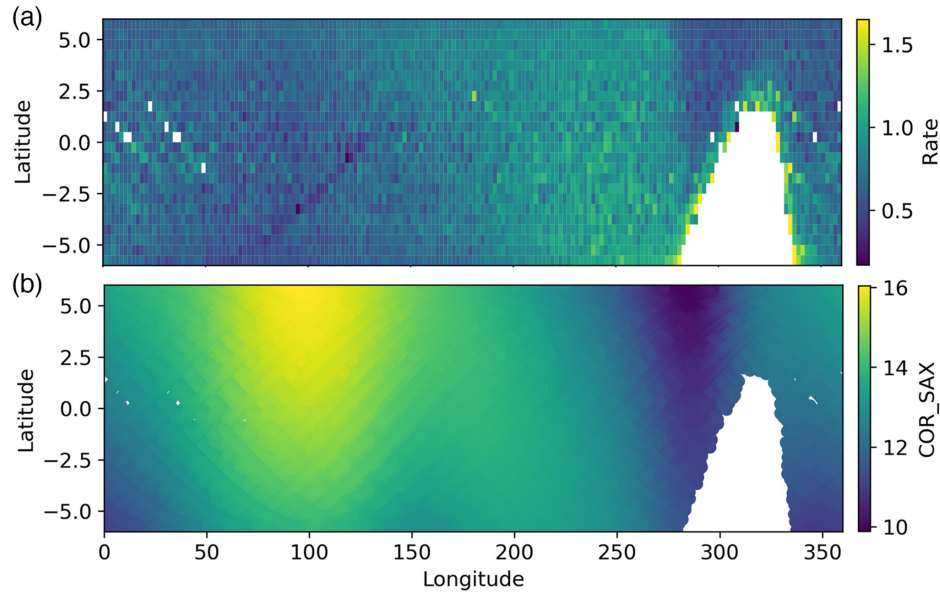


Fig. 7 (a) The geographic distribution of the *NuSTAR* background during April/May of 2019, a “quiet” period without significant solar activity. The blank area is when the instrument is in the SAA and the instrument stops recording data. (b) The apparent east/west variations are caused by the changes in the geomagnetic cutoff rigidity.

traces of the relevant geographic changes in the geomagnetic cutoff rigidity. The cutoff rigidity represents the ability of the Earth’s magnetic field to shield an instrument from cosmic rays, which are primarily responsible for the “flat” continuum background contribution.

We can instead project the background in the geomagnetic cutoff rigidity. This again is done using `prefilter` FTOOL, using the COR_SAX values, which are estimates of the local COR experienced by *NuSTAR* using the satellite ephemeris and three-dimensional geomagnetic field models.⁷ In this projection [Fig. 8(a)], we see that the structure of the background has a sharp drop around 11 GeV/c (implying that this is the location where *NuSTAR* is dipping above or below a radiation belt). We note that this dependence is different than that observed by *Suzaku*.⁸

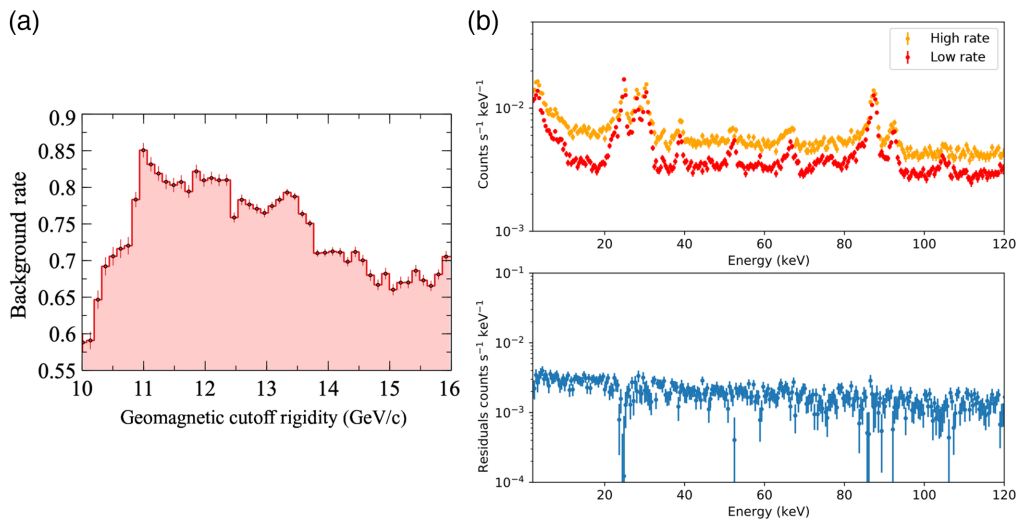


Fig. 8 (a) Count rates distribution versus geomagnetic cutoff rigidity for April/May of 2019 showing the ridge of excess emission around 11 GeV/c and the subsequent dropoff to lower cutoff rigidity values. (b) The spectrum from “high” and “low” backgrounds (top) and the residual background showing that (outside of a deficit near ≈ 25 keV) the additional background is largely a featureless power-law continuum.

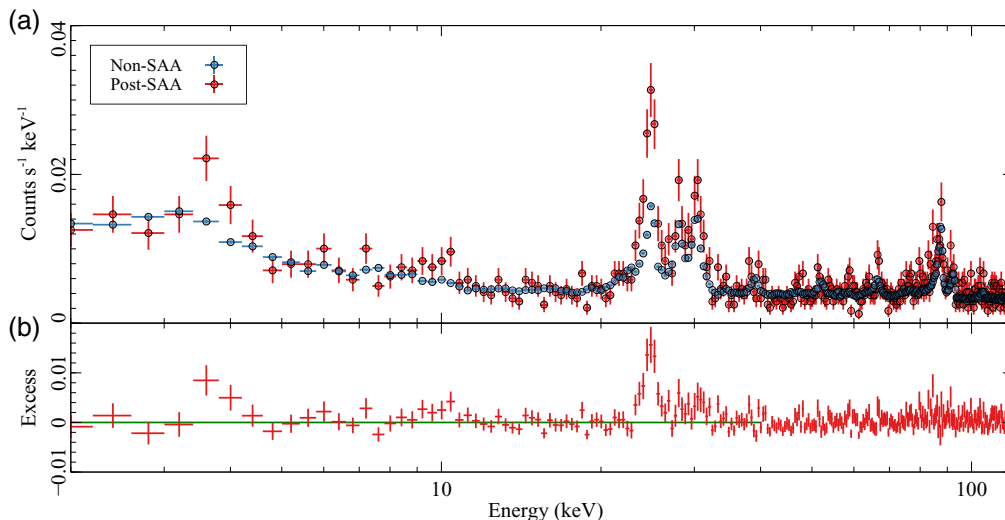


Fig. 9 (a) Spectrum extracted just after *NuSTAR* passes through the SAA (red) compared with the non-SAA spectrum (blue). (b) The residuals between the two spectra show a clear line at ≈ 25 keV and a broad excess at ~ 3.9 keV.

One explanation for this is that the two satellites are orbiting at different inclinations and different altitudes. This results in the two satellites traversing different regions of the geomagnetic field and the radiation belt structure.

3.1 SAA-Induced Radioactivity

There is spatial variation in a line emission near ≈ 25 keV, which is apparently related to activation of material in the CdZnTe detectors during the passages through the SAA. If we isolate the period of time just after the SAA passages and compare this with the total average spectrum, we clearly see the line (Fig. 9). To define this region we define the “radioactive” region as locations where the geomagnetic cutoff rigidity is between 10.8 and 12 GeV/c and the longitude of the satellite is above 320 deg. The “Non-SAA” spectrum shown in Fig. 9 is the average spectrum outside this geomagnetic and geographic location. The only other excess that we observe is a broad excess near 3.9 keV. There do not appear to be many (if any) other obvious SAA-induced activate lines. We checked with prelaunch simulations of activation in the *NuSTAR* instrument and cannot identify a likely counterpart for these line features (though these may possibly be related to isotopes of Cd). The orbital path through the SAA means that it is difficult to determine the decay timescale. For now, we simply note the presence of this line and that it can be time variable as an impact on empirical models of the *NuSTAR* background.

3.2 “The Tentacle”

One of the more common enhancements in the *NuSTAR* background occurs when *NuSTAR* passes through a short-lived radiation belt, which has been dubbed “the tentacle” due to its morphology in the *NuSTAR* ground maps stretching away from the SAA itself. This radiation belt appears after a CME passes nearby the Earth and can last for up to a week.

This excess background is fairly well localized geographically and geomagnetically (Fig. 10). Since 2013, versions of the NuSTARDAS software pipeline have included filtering mechanisms (via the `nucalcsaa` FTOOL) to flag and remove excess background in this region. There are a number of filter options that can be examined observation-by-observation using the *NuSTAR* background maps available at the SOC.

The spectrum [Figs. 10(c) and 10(d)] shows a uniform power-law excess across the band-pass, implying that this is also caused by an increase in the rate of charged particles. However, we do not see much excess emission near the CsI fluorescence lines (20 to 30 keV), or near any other radioactive lines across the band-pass.

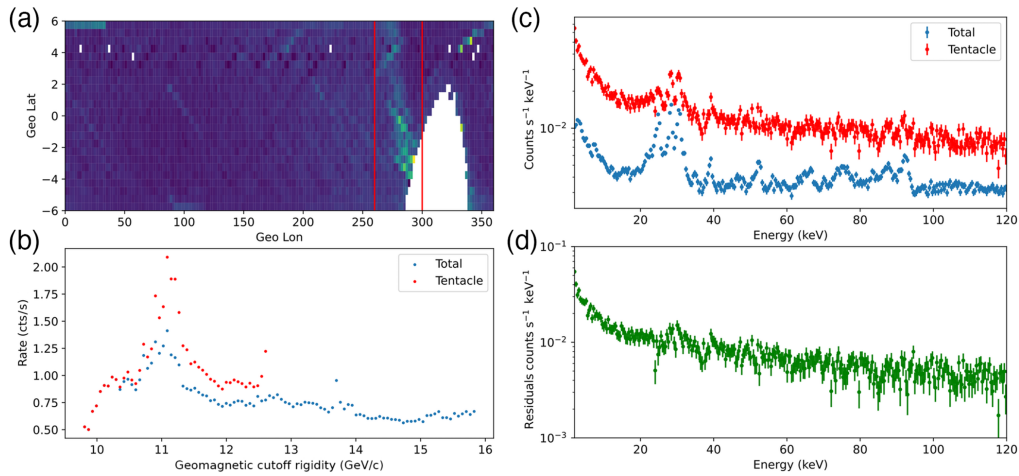


Fig. 10 (a) The *NuSTAR* >10 keV count rate, binned by the geographic sub-satellite point for a month's worth of data. The blank area between 270 deg and 320 deg longitude is the SAA, while the region between the vertical red lines shows “the tentacle.” (b) The background rate (integrated over DET0) versus geomagnetic cutoff rigidity for the total data (blue) and the data in the geographic tentacle region (red). (c) The total *NuSTAR* spectrum (blue) and the spectrum for the selected geographic and geomagnetic “tentacle” region (red) from 2 to 120 keV. (d) The excess emission in the tentacle region appears to be a relatively featureless power-law spectrum across the entire band-pass and does not appear to excite any activation lines in the detectors or the surrounding material.

NuSTAR passes through this region at most once per orbit, and during some orbits this may be when the primary *NuSTAR* target is occulted by the Earth. Fortunately, any apparent long-term (orbital timescale) periodic signals for astrophysical sources can be identified as spurious if they primarily occur in this region.

4 Long-Term Variations

4.1 Growth of Activation Lines

The high energy activation lines are dominated by the 88 and 92 keV lines, which we associate with isotopes of Cd. In particular, the 88 keV line shows growth on a yearly timescale (Fig. 11). However, this growth is non-monotonic and does show a plateau roughly during the period of

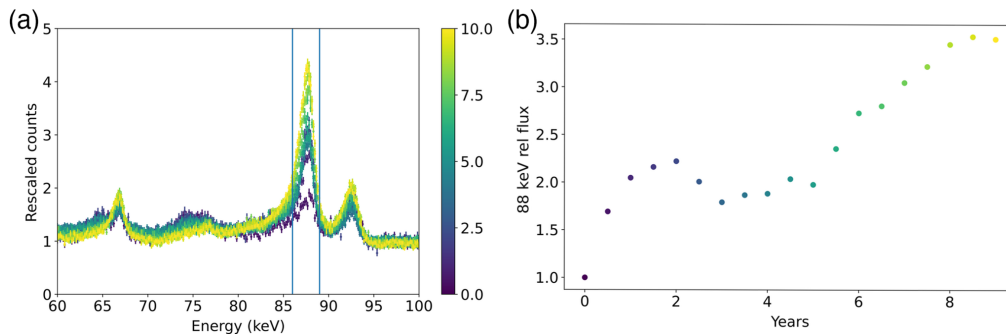


Fig. 11 (a) Six-month integrated spectra for FPMA (all detectors) showing the growth of the 88 keV line over time (color indicates years since launch). All epochs have been normalized by the count rate in the 110 to 120 keV line-free band to emphasize the change in the line strength relative to the underlying continuum. (b) The strength of the 88 keV line relative (integrated over the vertical lines in the left panel), normalized to the line strength in 2012 to highlight the growth of the line over time.

Table 1 The CdZnTe thickness for the eight detectors flying on *NuSTAR* as measured during ground testing.

FPM	DET	Hybrid	Thickness (mm)
A	0	H84	2.00
A	1	H95	1.66
A	2	H98	2.08
A	3	H94	1.63
B	0	H81	1.89
B	1	H80	2.01
B	2	H82	2.00
B	3	H75	2.00

solar maximum. This could be related to the changing particle background as the solar cycle interacts with the Earth’s magnetosphere. A similar trend is seen in the change in gain over time of the *NuSTAR* detectors.⁹ The time-dependent gain has already been accounted for in these data, but both effects may be related to the same underlying change in background particle flux.

4.2 Detector-to-Detector Variation

The four CdZnTe detectors on each focal plane have slightly different thicknesses, ranging from 1.5 to 2.0 mm (Table 1). The difference in detector volume can result in a change in the overall count rate between the detectors. All of the FPMB detectors are roughly the same thickness, so we see little variation between the detectors on that FPM. The FPMA detectors vary in thickness, resulting in more detector-to-detector variation. In the standard background model `nuskybgd`,² this variation is accounted for via a featureless power-law term with a normalization that varies by $\approx 5\%$ to 10% between detectors. We extract background spectra from 100 to 120 keV when the observatory is in orbital night and computed the monthly average count rate for all four detectors on each focal plane. We clearly see that beat frequency (not plotted) of the monthly integration windows with the precession period of the observatory; however, when we scale the count rates to be relative to DET0, we see no evidence for any time-dependence in the relative strength of the internal background continuum (Fig. 12).

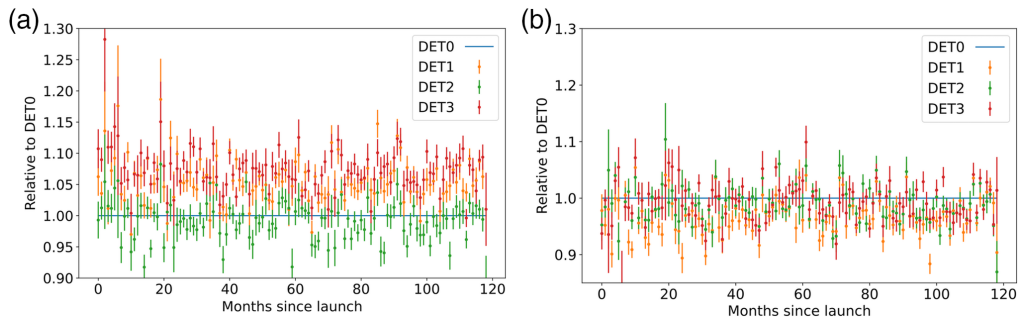


Fig. 12 Monthly average 100 to 120 keV count rate versus time for (a) FPMA and (b) FPMB relative to DET0 on both FPMs. No clear trends with time are seen in the relative strength of the internal continuum.

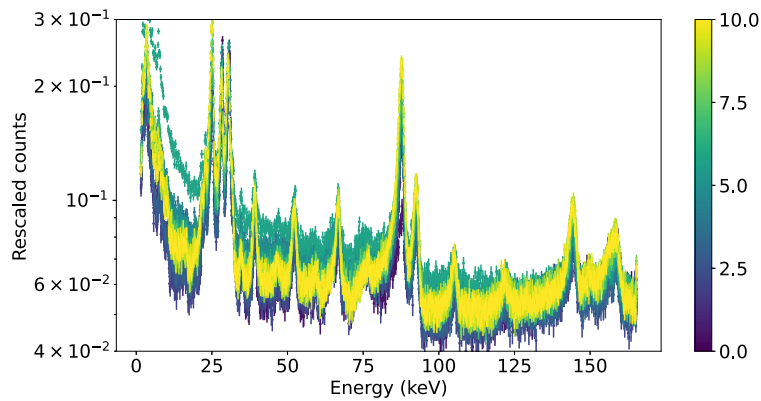


Fig. 13 Background spectra for FPMA (all detectors) integrated over 6-month intervals. Color indicates years-since-launch.

4.3 Variation in the Internal Continuum

The overall continuum shape has been relatively stable over time, with some deviations associated with high background periods associated with solar activity. We integrate the background in 6-month intervals to highlight the changes in the spectral shape (Fig. 13). While the shape is mostly stable, the overall normalization varies by roughly 50% between 6-month intervals.

5 Summary and Discussion

In this paper, we have investigated the origin and evolution of the non-x-ray background for *NuSTAR*. The dominant continuum components are associated with particle backgrounds and are modulated by the relative position of *NuSTAR* with respect to the Earth’s magnetic field. This evolves over time as the field responds to particle fluxes from the Sun. This generally manifests as a featureless continuum across the *NuSTAR* band.

Line features are associated with known activation lines. The relative line fluxes do not vary significantly, except for the 88 keV line, which has grown in strength over time, and the 24 keV line, which is a short-lived activation line and appears only when *NuSTAR* has recently passed through the SAA.

Additional short-term variations are generally associated with elevated solar activity. This can be seen in x-rays during solar flares (reflecting off the spacecraft or directly penetrating the shielding) or through the activation of short-lived radiation belts (the tentacle).

The original goal of this work had been to produce a “background database” of spectra, which could be used to generate a synthetic *NuSTAR* background spectrum (or background model) appropriate for any particular observation. There have been attempts to do this during the early parts of the mission, with varying degrees of success. In practice, the temporal variations discussed here suggest that the best approach is to simply model the background using the existing simulation tools (<https://github.com/NuSTAR/nuskybgd-py>). These are sufficiently flexible to fit for the observation-dependent radiation background (e.g., the strength of the featureless continuum) and the time-dependent strengths of the 24 and 88 keV lines.

Acknowledgments

This work was supported under NASA Contract No. NNG08FD60C, and made use of data from the *NuSTAR* mission, a project led by the California Institute of Technology, managed by the Jet Propulsion Laboratory, and funded by the National Aeronautics and Space Administration. This research has made use of the NuSTAR Data Analysis Software (NuSTARDAS) jointly developed by the ASI Space Science Data Center (SSDC, Italy) and the California Institute of Technology (USA). This material is based upon work supported by NASA under award number 80GSFC21M0002. We thank Dan Stern for constructive comments on this manuscript and

to the anonymous referees for their feedback. The authors have no relevant financial interests in the manuscript and no other potential conflicts of interest to disclose.

Code, Data, and Materials Availability

All data for this paper are publicly accessible via the *NuSTAR* repository in the High Energy Astrophysics Archive at NASA GSFC. Data were processed using the publicly available *nustardas* FTOOLS as described in this paper. All of the filtering and sorting steps are described in the text. Plots were produced using `matplotlib`¹⁰ in Python.

References

1. F. A. Harrison et al., “The nuclear spectroscopic telescope array (NuSTAR) high-energy X-ray mission,” *Astrophys. J.* **770**, 103 (2013).
2. D. R. Wik et al., “NuSTAR observations of the bullet cluster: constraints on inverse compton emission,” *Astrophys. J.* **792**, 48 (2014).
3. R. Krivonos et al., “NuSTAR measurement of the cosmic X-ray background in the 3-20 keV energy band,” *MNRAS* **502**(3), 3966–3975 (2020).
4. K. K. Madsen et al., “Observational artifacts of nuclear spectroscopic telescope array: ghost rays and stray light,” *J. Astron. Telesc. Instrum. Syst.* **3**, 044003 (2017).
5. B. W. Grefenstette et al., “StrayCats: a catalog of NuSTAR stray light observations,” *Astrophys. J.* **909**, 30 (2021).
6. T. Kitaguchi et al., “Spectral calibration and modeling of the NuSTAR CdZnTe pixel detectors,” *Proc. SPIE* **8145**, 814507 (2011).
7. HEASARC, “Prefilter documentation,” <https://heasarc.gsfc.nasa.gov/lheasoft/ftools/headas/prefilter.html> (2020).
8. N. Tawa et al., “Reproducibility of non-X-ray background for the X-ray imaging spectrometer aboard Suzaku,” *Publ. Astron. Soc. Jpn.* **60**, S11–S24 (2008).
9. B. Grefenstette et al., “Measuring the evolution of the NuSTAR detector gains,” (2022).
10. J. D. Hunter, “Matplotlib: a 2D graphics environment,” *Comput. Sci. Eng.* **9**, 90–95 (2007).

Brian W. Grefenstette is a research scientist at the California Institute of Technology and a member of the NuSTAR Science Operations Team. He received his BS degree in physics from Stanford in 2004 and his PhD in physics from the University of California, Santa Cruz, in 2009 and has been a member of the NuSTAR team at Caltech ever since.

Kristin K. Madsen received her PhD in astrophysics from the University of Copenhagen in 2007. She has more than 10 years of experience in x-ray optics and astrophysical research and is one of the principal instrument and mission scientists for NuSTAR. She currently works as a staff scientist at Goddard Space Flight Center. Her research interests include active galactic nuclei, x-ray binaries, pulsar wind nebulae, and hard x-ray optical design.

Hiromasa Miyasaka is a senior staff scientist at California Institute of Technology. He received his PhD in physics from Saitama University, Japan, in 2000. He has over 20 years of experience in development of particles and x-ray detectors for the cosmic ray and high-energy astrophysics. Since 2006, his work has focused on CdZnTe and CdTe detectors and readout ASIC development. He is one of the primary detector scientists for the NuSTAR mission.

Andreas Zoglauer received his PhD from the Technische Universität München, Germany, in 2005 for the development of novel simulation and data analysis tools for the MEGA telescope. He currently works at the University of California at Berkeley, and his research interests include the development of new simulation and analysis techniques, and the optimization and performance prediction of future instruments.